CHARACTERIZATION OF THE ABRASION RESISTANCE AND THE ACOUSTIC WAVE ATTENUATION OF THE ENGINEERED CEMENTITIOUS COMPOSITES FOR RUNWAY PAVEMENT

Chao Wu [1,*], Yang Pan [1], Tamon Ueda [2]

[1] School of Transportation Science and Engineering, Bseihang University, 37 Xueyuan Road, Beijing 100191, China

[2] Division of Engineering and Policy for Sustainable Environment, Faculty of Engineering, Hokkaido University, Kita 13 Jo Nishi 8 Chome Kita-ku, Sapporo 060-8628, Japan

**Corresponding author E-mail: wuchao@buaa.edu.cn*

ABSTRACT

Concrete runway pavement is subjected to a critical issue of brittle cracking, which is hazardous for the safety operation of the airport. Engineered cementitious composite (ECC) is a promising pavement material due to its ductility with a strain capacity up to 5%, as well as its desirable micro-cracking and self-healing properties. However, the abrasion resistance and acoustic wave attenuation of ECC, which are important behaviors for a pavement, have not been quantified yet. This paper presents an experimental program to investigate the abrasion resistance and the acoustic wave attenuation of ECC. The experimental results showed that the abrasion resistance of ECC (with 3% fiber volume ratio) could be comparable with the ordinary concrete of the same compressive strength. It was also found that, the acoustic wave attenuation

of ECC was positively related with its fiber volume ratio and much higher than that of the ordinary concrete with the same compressive strength. It was interesting to find that the acoustic wave attenuation of ECC was independent of the wave frequency (ranging from 200 Hz to 2000 Hz) of the acoustic signal. The underlying mechanisms for the abrasion resistance and acoustic wave attenuation of ECC were discussed with the measurement of its void ratio, compressive and tensile properties.

KEYWORDS: Abrasion resistance; Acoustic wave attenuation; Engineered cementitious composites (ECC); Pavement

1. INTRODUCTION

Many international airports have adopted concrete runway pavement due to its high strength and stiffness with low surface deformation [1-3]. However, the concrete pavement has an inherent drawback of brittle cracking, which is hard to repair and limits the service life of the pavement [2, 4, 5]. The debris from the cracking may also damage the engine of the airplane which raises a critical issue for the safety operation of the airport. Recently, engineered cementitious composite (ECC) has been proposed as the road pavement by many researchers [6-9]. ECC was developed based on the micro fracture mechanics with a strain capacity in the range of 3–7% [10], comparing to 0.1% for ordinary concrete. This ductility of ECC is achieved by micro-cracking (with micro-crack width less than 100 mm [10]) in the strain hardening stage [11]. Considering these advantages, ECC is a promising alternative to the conventional concrete pavement. This can be demonstrated by a pioneer project using ECC as a

link slab of a bridge located in southeast Michigan, US [12].

However, before more pavement applications of ECC, many other important properties have to be characterized such as the abrasion resistance [13, 14], acoustic wave attenuation [15, 16] and etc. This is to ensure that ECC is qualified in every aspect to be used as a pavement material. Unfortunately, the abrasion resistance of ECC has scarcely been reported in the literature [17, 18], although this property of the other fiber reinforced concrete has been widely researched. For ordinary concrete, many factors could affect the abrasion resistance, such as the environmental conditions, the cement to sand ratio, the use of special cement or supplementary cementitious materials, etc. [19-27] As for the polyester fiber reinforced concrete, its abrasion resistance increased when more polyester fibers (0.03%-0.14% volume ratio) were added in the mixture [28-30]. However, the above findings on the abrasion resistance of the concrete or fiber reinforced concrete materials may not be directly applicable to the ECC. This is because ECC has different mixture and microstructure. For example, ECC has no coarse aggregate in the mixture, and it uses silica sand with a maximum grain size of 250 μm which is much finer than the sand in the concrete [31-35]. In addition, the volume ratio of Poly-Vinyl Alcohol (PVA) fibers in ECC is around 2%, which is about 20 times higher than the fiber volume ratio of the fiber reinforced concrete [28-30]. Therefore, the abrasion resistance of ECC needs to be investigated to be used as the pavement material.

The acoustic wave attenuation is another important property of the pavement because it is related to the noise reduction when the tyres are running on the pavement

surface. The pavement is expected to absorb as much noise as possible to limit the interference to the passengers [16] and surrounding environment. However, there has been little research on the characterization of the acoustic wave attenuation of ECC in the literature. This is probably due to the lack of suitable international testing standard to characterize and compare the acoustic wave attenuation among different pavement materials. ISO 11819-1:1997 describes several methods for the measurement of the pavement noise, such as Statistical Pass-By method [36], Close-proximity method [37], Reference tyres [38] and SPB method using backing board [39]. However, these methods require building a 100-meter long road with the vehicle running on the pavement and at the same time measure the noise with on-board complicated acoustic facilities [36-39]. Therefore, it is necessary to develop a testing method which is suitable and convenient to be conducted in the laboratory scale to compare and select among different pavement materials. It has been reported that the acoustic frequency generated between the tires and the pavement ranges between 200 Hz and 2000 Hz [15], i.e. 600 Hz for low-speed road, and 1000 Hz for the high-speed road [15]. Considering these acoustic behaviors, the routine ultrasonic testing method in the structural health monitoring can be resorted to characterize the acoustic wave attenuation of the pavement materials [41-43]. The details and setup of this method will be introduced in the experimental program of this paper.

This paper presents an experimental program to characterize the abrasion resistance and the acoustic wave attenuation of ECC. Specimens of ECC with a fiber volume ratio from 1% to 5% were prepared and tested. For comparison purpose, ECC

matrix specimens without fibers and the ordinary concrete specimens with the same compressive strength as the ECC specimens with a fiber volume ratio of 2% were also tested. The abrasion tests were conducted and the index of abrasion resistance of ECC and concrete were calculated. A new method for the characterization of the acoustic wave attenuation of ECC and concrete was developed. Finally, the abrasion resistance and acoustic wave attenuation of ECC was discussed considering the compressive and tensile properties as well as the void ratio of the material. This paper contributes to the understanding on the abrasion resistance and acoustic wave attenuation of ECC for pavement applications.

2. EXPERIMENTAL PROGRAM

2.1 Materials and Mix Proportions

ECC specimens with various fiber volume ratios were prepared. The mix proportions of the ECC specimens are presented in Table 1. The name of specimens was denoted using the form of “E-N”, where “E” refers to ECC and “N” means the percentage of the fiber volume ratio. The mixture of E-2 was intentionally designed to generate strain hardening and microcracking behaviors according to the micro fracture mechanics [44-46]. While other ECC specimens had the same mix except changing PVA volume ratios.

The raw materials in the mixture of ECC include ordinary Portland cement (P.O 42.5), fly ash, fine aggregate (F-75 silica sand), water, olycarboxylate-based high range water reducing admixture (HRWRA) and the Poly-Vinyl Alcohol (PVA) fibers.

Ordinary Portland cement was provided by BBMG Cement Trading Co., LTD, and the chemical properties provided by the manufacturer are listed in Table 2. The fly ash was from Lingshou Country, Lanxiang Mineral Processing Plant with the chemical compositions shown in Table 3. The F-75 silica sand from Huiyan Mineral Processing Plant has a maximum grain size of 250 μm and an average grain size of 110 μm. HRWRA provided by Sobute New Materials Co., LTD was used. The PVA fibers were purchased from Kuraray Trading Co., LTD and the detailed properties are summarized in Table 4.

For comparison purpose, the concrete specimens (C) with similar compressive strength to that of E-2 were also prepared based on JGJ 55-2011 [47]. The mix proportion of the concrete is presented in Table 5. The chemical properties of the ordinary Portland cement (P.O 32.5) provided by the manufacturer are listed in Table 2. It should be noted that the cement of P.O 32.5 was used for concrete specimens and the purpose was to prepare concrete specimens with similar compressive strength to the E-2. River sand was used in the mixture with a fine modulus of 3.0. The grain size of the coarse aggregate was between 5 mm to 20 mm.

Table 1. The mixture of the ECC specimens

No.	Water (W) (kg/m^3)	Cement (C) (kg/m^3)	Fly ash (FA) (kg/m^3)	Silica sand (kg/m^3)	PVA fiber		HRWRA kg/m^3	W/(C+FA) Ratio	FA/C Ratio
					By weight (kg/m^3)	By volume (%)			
E-0	457	306	969	510	0	0	0.5	0.39	4.7
E-1	453	303	960	505	13	1	1.6	0.39	4.7
E-2	449	300	950	500	26	2	3.3	0.39	4.7
E-3	444	297	940	495	39	3	5.0	0.39	4.7
E-4	440	294	931	490	52	4	6.7	0.39	4.7
E-5	435	291	921	485	65	5	8.3	0.39	4.7

Table 2. The chemical properties of the ordinary Portland cements (P.O 42.5 and P.O 32.5)

Composition	SiO_2	Al_2O_3	Fe_2O_3	CaO	MgO	C_3S	C_2S	C_3A	C_4AF
P.O 42.5	22.09	5.13	3.79	66.33	1.96	55.62	23.37	6.96	12.39
P.O 32.5	20.33	5.31	4.13	67.21	1.91	57.27	18.31	8.05	12.41

Table 3. The chemical composition of the fly ash

Composition	SiO_2	Al_2O_3	Fe_2O_3	CaO	MgO	SO_3	Na_2O	K_2O	Loss on ignition
The fly ash	50.8	28.1	6.2	3.7	1.2	0.8	1.2	0.6	7.9

Table 4. The properties of the PVA fiber

Diameter (μm)	Length (mm)	Nominal strength (MPa)	Modulus (GPa)	Density (kg/m^3)
40	12	1560	41	1300

Table 5. The mixture of the concrete specimens (kg/m^3)

Cement	Sand	Stone	Water
490	590	1100	220

2.2 Specimen Preparation

The ECC specimens were prepared in a B20 mixer of 20 L capacity (Henglian Food Machinery Co., LTD). Firstly, the cement, fly ash and silica sand were dry mixed for 5 min at a speed of 168 r/min. Then the mixture of water and HRWRA was gradually added and mixed for another 10 min under the same speed. Then the PVA fibers were slowly added into the mortar and mixed for 8 min at a speed of 400 r/min. The mixture was checked for fiber agglomeration. Finally, the mixing continued for

another 2 min until the fibers were well dispersed. The preparation process was the same for E-0 without adding PVA fibers.

The concrete was prepared in a HJW-60 mixer of 60 L capacity (Cangzhou Kexing Instrument Co., LTD). The cement, sand and stone were dry mixed for 5 min at the speed of 48 r/min and then the water was added and mixed for another 10 min under the same speed.

For both the ECC and concrete specimens, they were firstly cured in the molds sealed with plastic bags and subsequently demolded after curing for 1 day. All specimens were cured for another 27 days in air under a temperature of 20 ℃± 3 ℃, and a humidity of 30 %± 5% RH. The air temperature and humidity were recorded by a digital thermometer and hygrometer (model HTC-1) from Zhengzhou Boyang Instrument and Meter Co., Ltd.

Different types of specimens were prepared for both ECC and concrete. Cubic specimens with a dimension of 100×100×100 mm^3 were used for the testing of the compressive strength [48] and the total void ratio. Dogbone-shaped specimens were prepared for the tensile testing. The detailed dimensions of the dogbone-shaped specimens can be found in the recommendations by the Japan Society of Civil Engineers (JSCE) [49]. Cubic specimens with a size of 150×150×150 mm^3 were prepared for the abrasion tests [50]. 50×50×350 mm^3 beam specimens were prepared for the characterization of the acoustic wave attenuation of both ECC and concrete [51]. The reasons for the selection of the above dimensions of the specimens will be discussed in the following texts.

2.3 Physical and Mechanical Testing

The compressive strengths of ECC and concrete were determined using three identical 100×100×100 mm^3 cubic specimens for each mixture according to GB/T 50081-2002 [48]. The compressive tests were conducted at a speed of 1 mm/min using a WAW-C universal testing machine from Ji'Nan Docer Testing Machine CO., LTD with a capacity of 2000 kN.

Fig. 1. The set-up of the compressive test

The tensile test of ECC was performed using dogbone-shaped specimens according to the JSCE Recommendations [49, 52]. The tests were carried out at a speed of 1 mm/min using an SANS-50kN electronic universal testing machine from Shenzhen SUNS Technology Stock CO., LTD. The experimental set-up is shown in Fig. 2.

Fig. 2. The set-up of the tensile test

The total void ratio of ECC and concrete specimens was determined with 100×100×100 mm^3 cubic specimens according to the JCI Test Method [53]. The 28-day cubes have been dried for 1 day under 105 ℃ with a DHG-9023A drying oven (Shanghai Dute Scientific Instrument Co,. LTD). And the mass of the cube was tested. Then the cubes were dried under the same condition for another 2 hours, and the mass of the cube was tested again and it did not change. Then the cubes were considered as fully dried. The mass (M_1) of the fully dried cube was firstly weighed. Then the cube was immersed in the water for 1 day, after which the wet cube was taken out and the surfaces were wiped using dry cloth. The mass (M_2) of the wet cube was then recorded. The total void ratio (A) can be determined by:

$$A = \frac{M_2 - M_1}{\rho_{water} \cdot V_{specimen}} \quad (1)$$

where, ρ_{water} is the water density and $V_{specimen}$ is the cube volume.

2.4 Abrasion Testing

The abrasion tests were conducted according to the standard of "Test method for abrasion resistance of concrete and its products (GB/T 16925-1997) [50]" using a standard abrasion machine TMS-04 from Wuxi Jianyi Instrument & Machinery CO., LTD. Cubic specimens with a dimension of 150×150×150 mm^3 were prepared which could fit in the abrasion machine. The test set-up is shown in Fig. 3(a). The abrasion head firstly pressed on the top surface of the specimen with a pressure of 200 N. Then the head rotated at a speed of 630 r/min. After a number of revolutions, the abrasion head would cut in the material leaving a circular abraded area on the top surface of the specimen (Fig. 3b). The depth of the abraded area was measured using a dial indicator. The readings at the four locations of "a", "b", "c", "d" in Fig. 3(b) were taken and averaged to represent the depth of the abrasion corresponding to the specific number of revolutions. The test stopped when the depth of the abraded area reached 1.5 mm (the maximum depth that the machine could achieve). The abrasion resistance of the material can be represented using the following index:

$$I_a = \frac{\sqrt{\mathrm{R}}}{\mathrm{P}} \quad (2)$$

where, I_a is the index of abrasion resistance, R is the number of revolutions of the abrasion head (thousand revolution), P is the total depth of the abraded area corresponding to the number of revolutions R [50]. It should be noted that, the index of the abrasion resistance was determined on three identical specimens for each

mixture.

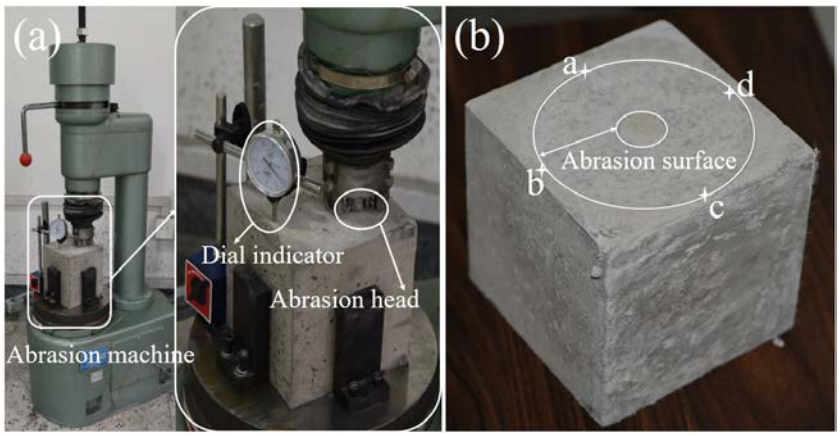

Fig. 3. (a) The set-up of the abrasion test and (b) the locations for the measurement of the abrasion depth

2.5 Acoustic Testing

As mentioned in the introduction section, the current available method for the measurement of the acoustic properties of the pavement requires building a 100-meter long road, which is impractical and uneconomic when numerous tests are necessary for the selection of pavement materials. In this paper, an ultrasonic testing method, which is a routine in the structural health monitoring field and convenient to set-up in the laboratory scale, is resorted to characterize and compare the acoustic wave attenuation of ECC and concrete for the pavement applications. The test set-up in Fig. 4 consists of a signal generator (model: RIGOL DG1022U, from Rigol Technologies, Inc.), an oscilloscope (model: Tektronix DPO2014 from Tektronix, Inc.), and three acoustic sensors (wide-band from 20 Hz to 20 kHz, model: GU14095A0 from

237 Dongguan Inghai Electronic Co., Ltd). One sensor was used as signal transmitter and
238 the other two were used as signal receivers A and B in Fig. 4. The transmitter,
239 receivers A and B were settled along the center line of the top surface of the beam
240 specimen. Receiver A was used to record the original signal from the transmitter, so
241 they were set by 10 mm away from each other to reduce the signal lost between the
242 two. Receiver B was used to record the residue signal from the transmitter after the
243 acoustic energy was partially absorbed by the pavement. The distance between
244 receivers A and B were set 35 mm to simulate the thickness of the pavement. In the
245 acoustic tests, the signal generator and the transmitter would generate the acoustic
246 waves with a frequency of 200 Hz, 400 Hz, 600 Hz, 800 Hz, 1000 Hz, 1200 Hz, 1400
247 Hz, 1600 Hz, 1800 Hz, 2000 Hz, respectively. For each specific frequency, receivers
248 A and B along with the oscilloscope would collect the amplitude of the acoustic wave
249 separately. The acoustic wave attenuation of the material can then be calculated as
250 [54]:

251 $$\Delta = 20\lg(A_1/A_2) \quad (3)$$

252 where, Δ is a representative parameter for the acoustic wave attenuation of the
253 material with a unit of dB/mm, A_1 (in mV) is the amplitude of the acoustic wave
254 before absorption recorded by receiver A, A_2 (in mV) is the amplitude of the acoustic
255 wave after absorption collected by receiver B. A brief schematic diagram was shown
256 in Fig. 4 to describe how the acoustic wave attenuation of the materials were
257 measured. For each mixture, the test was performed on three identical specimens for
258 repeating purpose.

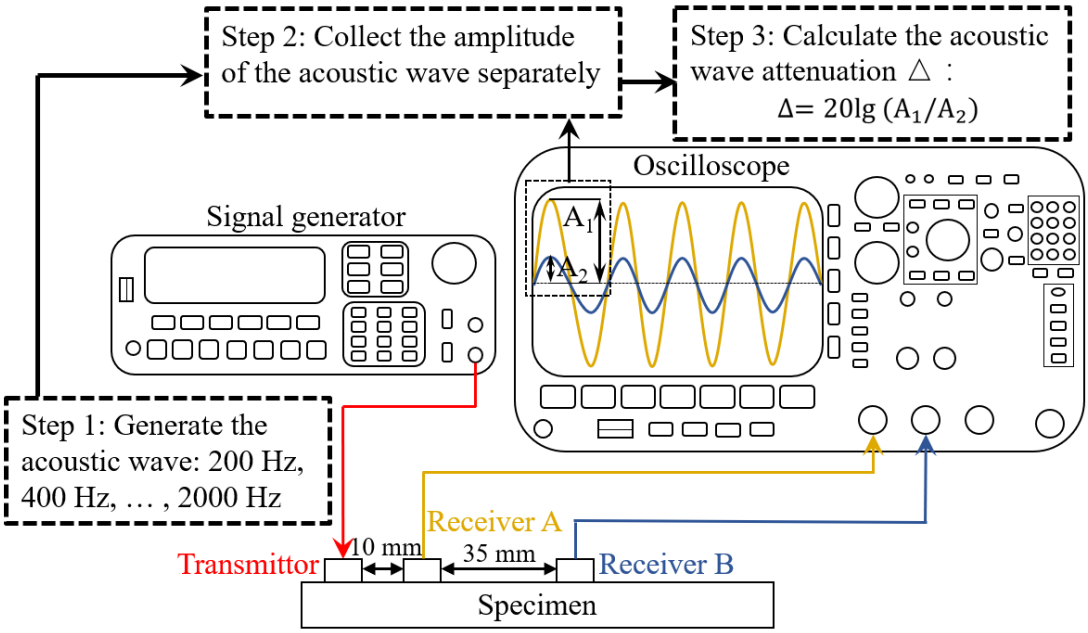

Fig. 4. The set-up and schematic diagram of the acoustic wave attenuation test

3. EXPERIMENTAL RESULTS AND DISCUSSIONS

3.1 The Physical and Mechanical Properties

3.1.1 Fiber dispersion of ECC with various fiber contents

Since ECC specimens with various PVA fiber volume ratios were prepared, it is important to ensure no fiber glomeration exists in the matrix. The ECC specimens were cut into thin pieces and observed using XSP-12CA optical microscope (Shanghai Optical Instrument Factory) with a magnification of 4 times. The microscope images of the ECC specimens with various fiber volume ratios are presented in Fig. 5. The black areas in Fig. 5 represent the cementitious matrix and the white parts are PVA fibers. It can be seen that, no PVA fiber glomerations can be noticed in all ECC specimens.

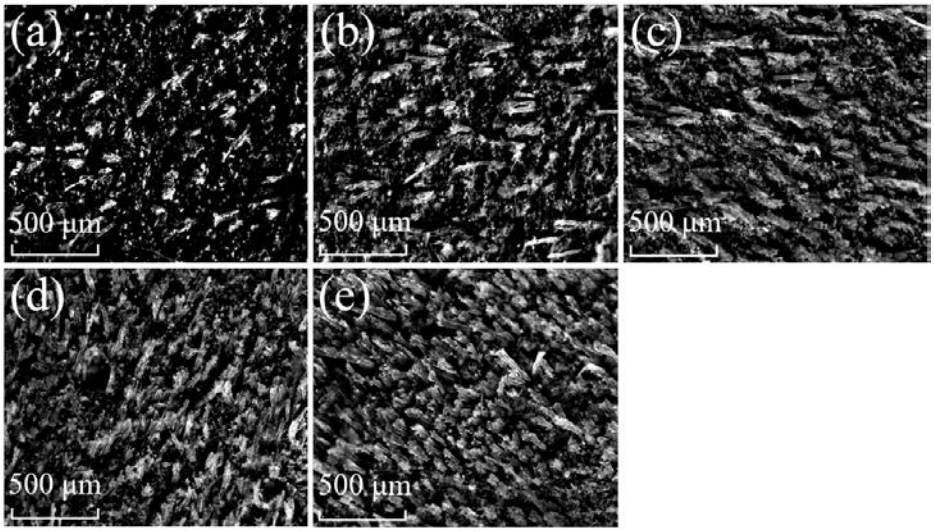

Fig. 5. The images of the ECC specimens with various fiber volume ratios (a) E-1; (b) E-2; (c) E-3; (d) E-4; (e) E-5

3.1.2 The void ratio of the ECC and the concrete specimens

The void ratios of the ECC and the concrete specimens are shown in Fig. 6. For ECC specimens, the void ratio increased with the fiber volume ratio. The void ratio of E-0 without fibers was the lowest as 1.93%. And when the fiber volume ratio increased to 1%, 2%, 3%, 4%, 5%, the void ratio was 2.10%, 2.40%, 2.56%, 2.81%, 3.21%, respectively. The void ratio of the ordinary concrete, used for comparison, was 1.83%, which was 0.09% lower than E-0.

Fig. 6 shows that the void ratio of the ECC specimens is dependent on the corresponding fiber volume ratio. For both concrete and ECC, there can be three kinds of pores generated: the capillary pores, the gel pores and the microcracks (i.e. the pores between different interface) [55]. The void ratio of the capillary pores, gel pores

was dependent on the water-cement ratio [56, 57]. As in Table 1, the water-cementitious material ratio of the ECC specimens was the same (0.39), the capillary pores and the gel pores could thus be similar between ECC specimens. When more fibers were added in the ECC mixture, this could contribute to the increase of the void ratio because more microcracks could be seen between the smooth fibers and the surrounding matrix in the SEM images of many studies [58, 59]. This might be the reason that the higher total void ratio could be achieved for ECC specimen with larger fiber volume ratio.

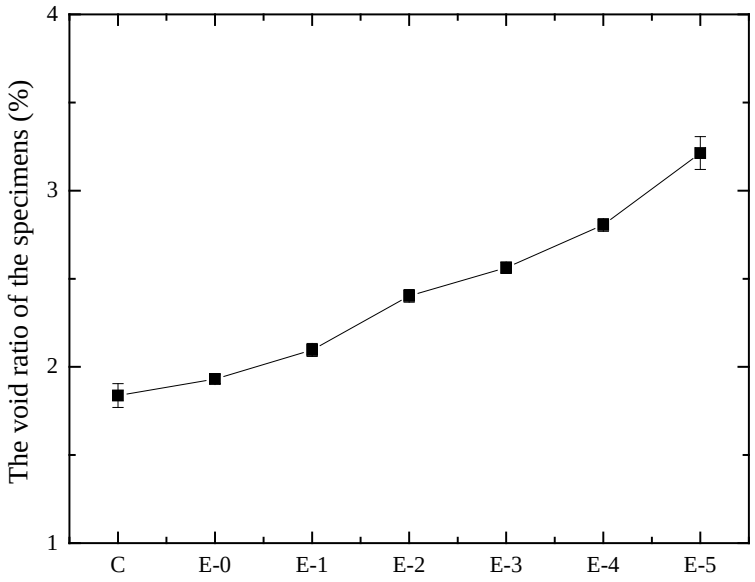

Fig. 6. The void ratio of the ECC and concrete specimens

3.1.3 The compressive strengths of the ECC and the concrete specimens

The 28-day compressive strengths of the ECC and the concrete are shown in Fig. 7. It can be seen that the compressive strength of ECC is highly dependent on the volume

ratio of the PVA fibers. For ECC matrix without fibers (E-0), the compressive strength was 20.33 MPa. With the increase of fiber content to 3%, ECC achieved the maximum compressive strength of 34.13 MPa, showing a 68% increase comparing to E-0. When more fibers were added, the compressive strength of ECC was negatively affected, i.e. the compressive strength of E-5 decreased to 25.28 MPa (26% less than that of E-3). It can be seen that ECC could achieve comparable compressive strength to concrete when the mixture of ECC is carefully designed.

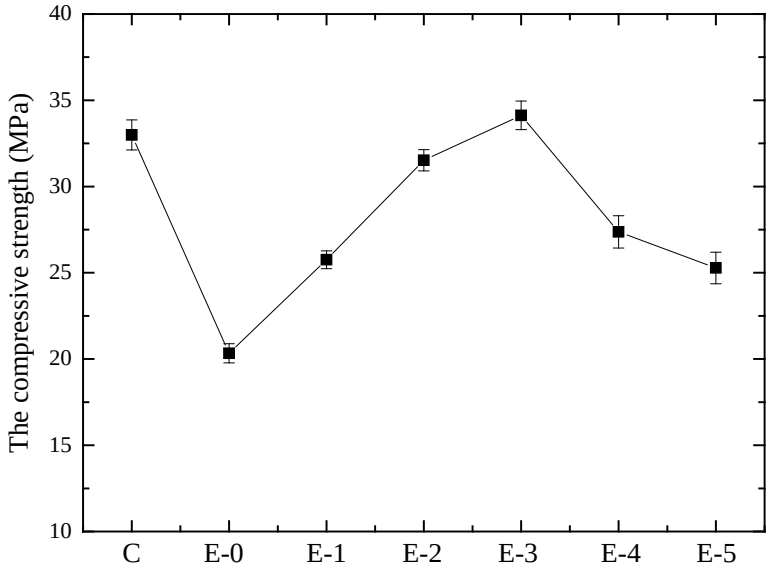

Fig. 7. The compressive strength of the ECC and concrete specimens

It has been reported that the fiber content may affect the compressive strength of the fiber reinforced concrete [60, 61]. For E-0 without PVA fibers, the compressive strength was merely dependent on the structure network of the hydrate of the cementitious material [56, 62, 63], i.e. E-0 would break with a single crack rapidly under compression. When 1% fibers were added, the fibers could delay the crack

development, resulting in an increased compressive strength. With 3% PVA fibers, the highest compressive strength was achieved which could probably because the combined effects of the fiber-network and the structure network of the hydrate reached an optimum status. However, when more fibers (e.g. 4%, 5%) were added in ECC, the amount of the hydration product which contributes to the strength was reduced due to the decrease of the cementitious material and increase of the too much fibers in the mixture. For a cube of the same volume, the strength reduction was due to the combined effects of decreased cementitious material and increased fiber content. Because the addition of the fibers brought more interface between the fibers and the cementitious material. The decreased cementitious material had to bond more surface of the fibers which lowed the bonding of the particles of ECC. So the strength of the ECC was decreased. This is evidenced by the reduced compressive strength of E-4 and E-5 showing 19.8% and 25.9% strength reduction comparing to E-3.

3.1.4 The tensile properties of the ECC specimens

The tensile stress-strain curves of ECC with different fiber contents are shown in Fig. 8 (a). The first crack strengths of the ECC specimens are presented in Fig. 8 (b). It can be seen that the trend of the first crack strength of ECC was the same as that of the compressive strength in Fig. 7. The mechanism can be referred to the discussions in Section 3.1.3. Only E-2 shows strain hardening behavior with a strain capacity of 3.2%, while other ECC specimens experienced brittle failure with a strain capacity of only about 0.10%. The failure modes of ECC specimens are presented in Fig. 9, with E-2 exhibited multi cracking behavior and other ECC specimens failed by a single

crack. This is because E-2 was intentionally designed to show strain hardening and microcracking behaviors, while the other ECC specimens did not satisfy the requirements of the micro fracture mechanics as specified in [45, 46].

The area under the stress-strain curve in Fig. 8(a) is a suitable measurement of the energy absorbing capacity of ECC. The area under the stress strain curve was calculated by $\sum\sigma_i(\varepsilon_{i+1}-\varepsilon_i)$ where σ_i is the ith experimental stress data corresponding to the ith strain data of ε_i on the curve. This parameter was calculated and plotted in Fig. 8(b) comparing with the first crack strength of ECC with different fiber contents. It can be seen that, E-2 has the largest area under the stress-strain curve due to its strain-hardening behavior, while other ECC specimens exhibit much lower area values. For example, the area of the stress-strain curve of E-2 is 0.111 MPa which is almost 50 times higher than that of other ECC specimens (around 0.002 MPa). This indicates that E-2 could absorb extraordinary energy during the tensile cracking process.

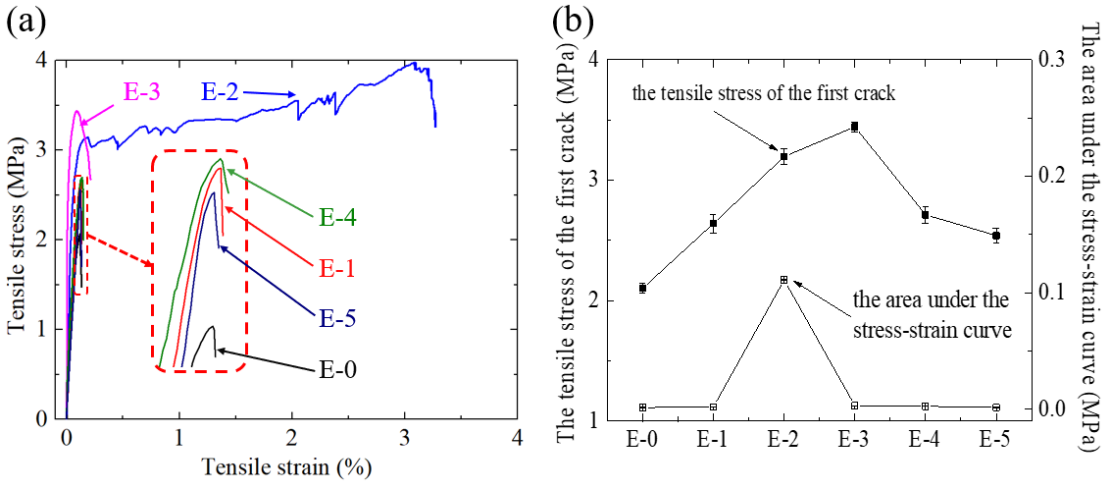

Fig. 8. (a) The stress-strain curves of the ECC specimens and (b) The first crack strength and the area under the stress-strain curve of the ECC specimens

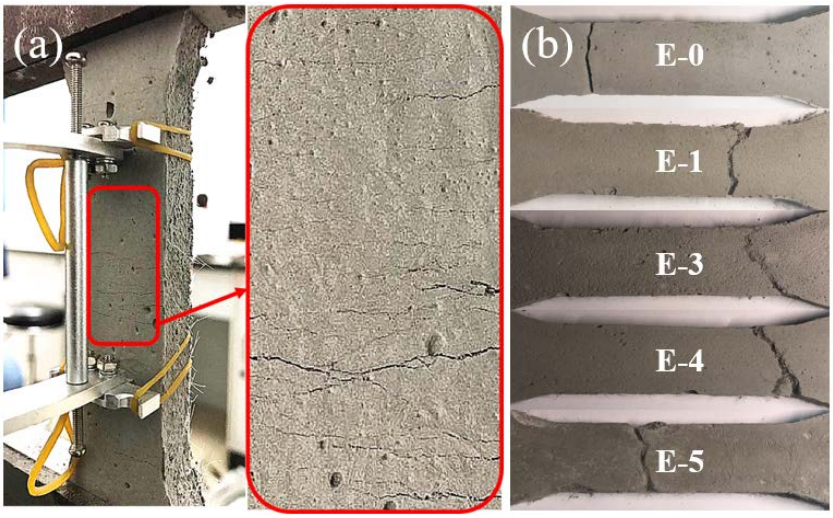

Fig. 9. Failure modes of (a) E-2 with multi cracking and (b) E-0, E-1, E-3, E-4, E-5 with a single crack

3.2 The Abrasion Resistance of the ECC and Concrete Specimens

The abraded areas of the ECC and concrete specimens were examined after the abrasion tests as shown in Fig. 10. The surface of the abraded area was also enlarged and presented in Fig. 10 to show more details. For the ECC specimens, only dust was generated during the abrasion test because no coarse aggregates were in the mixture. On the other hand, concrete specimens produced not only dust but also stone debris which was knocked off the surface by the abrasion head. When used as pavement, this debris from concrete may hazardous for the engine of the airplane, and the other road users. Therefore, ECC may provide a safe solution to the concrete pavement when other mechanical properties like compressive strength were comparable to the concrete. It is also obvious in Fig. 10, that more PVA fibers were exposed on the

abraded surface with the increase of the fiber volume ratio of ECC specimens. The uniformly distribution of the PVA fibers on the abraded surfaces of ECC specimens in Fig. 10 is another evidence of the well dispersion of these fibers in the matrix.

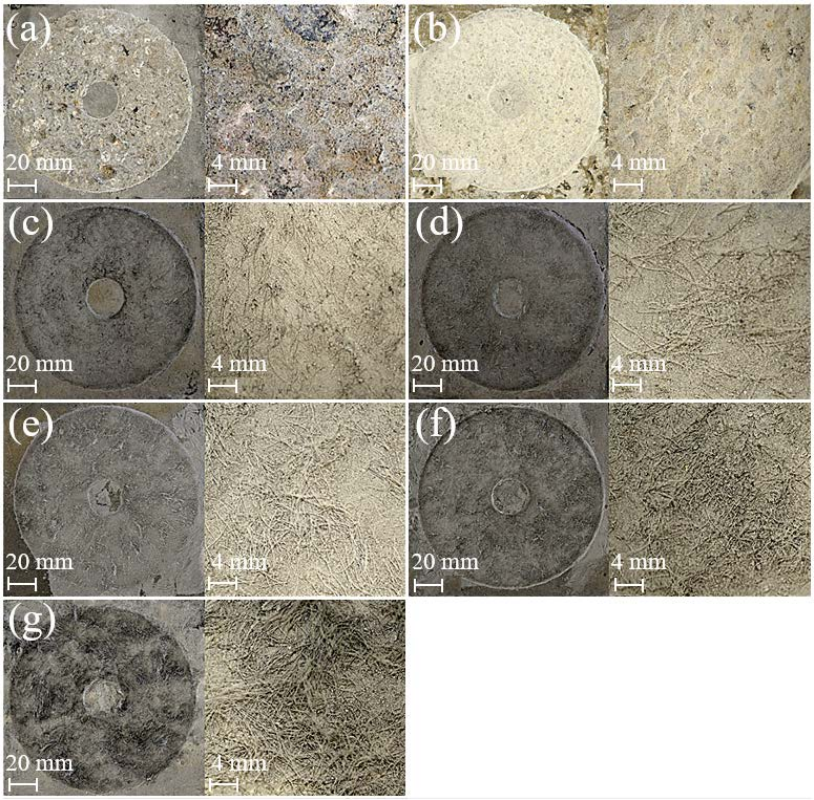

Fig. 10. The abraded surfaces and corresponding enlarged details of the (a) Concrete; (b) E-0; (c) E-1; (d) E-2; (e) E-3; (f) E-4; (g) E-5 specimens

The development of the abrasion depth was measured and plotted against the corresponding number of revolutions of the abrasion head for each specimen in Fig. 11. For the same abrasion depth, the ECC specimens required different number of revolutions depending on the fiber volume ratio, i.e. E-3>E-2>E-4>E-5≈E-1>E-0. Therefore, Fig. 11 can be used to qualitatively evaluate the abrasion resistance of ECC.

That is ECC matrix without fibers (E-0) has the lowest abrasion resistance while ECC achieved the best abrasion resistance when the fiber content was 3% (E-3).

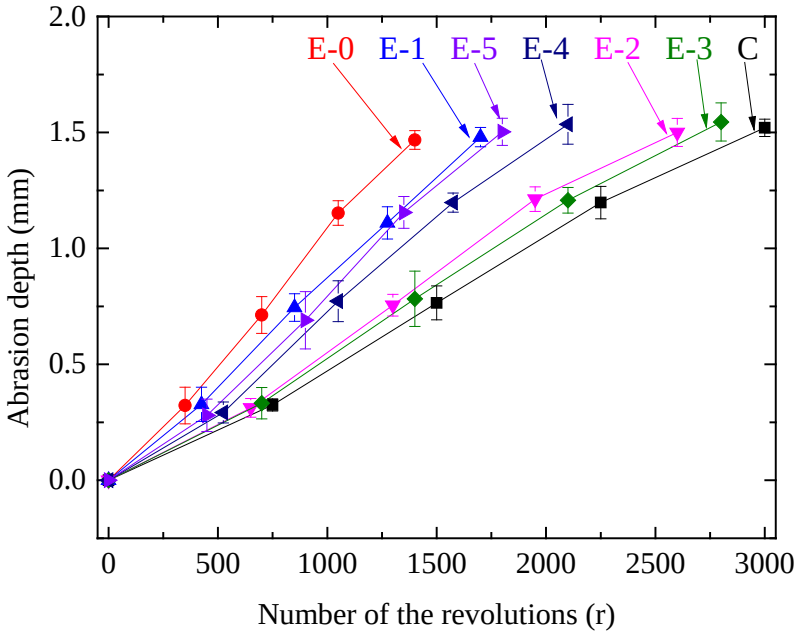

Fig. 11. The abrasion depth versus the number of revolutions of the abrasion head for the ECC and concrete specimens

The indexes of the abrasion resistance of the ECC and concrete specimens were calculated using Eq. 2 and were presented in Fig. 12. For ECC specimens, there seems an optimum fiber content to achieve the maximum abrasion resistance. The abrasion resistance of ECC was the lowest with an index of 0.79 when there was no fiber in the mixture (E-0). The abrasion resistance increased to 0.87 with a fiber content of 1% (E-1), and 1.05 for E-2. When 3% volume ratio of the PVA fibers were added in the mixture, the abrasion resistance reached the maximum of 1.09 for E-3. However, when more PVA fibers were added, the abrasion resistance of ECC

404 decreased, i.e. to 0.93 and 0.88 at 4% and 5% fiber volume ratios respectively. The
405 index of the abrasion resistance of the concrete (1.15) is a little higher than E-3 (1.09).
406 It is important to notice that the trend of the index of the abrasion resistance
407 of ECC is the same as the trend of the compressive strength in Fig. 7 and the tensile
408 strength in Fig. 8(b). This indicates the abrasion resistance of ECC is highly
409 dependent on its compressive and tensile strengths. It seems that the energy
410 absorption capacity of ECC in Fig. 8(b) has little effect on its abrasion resistance. This
411 is understandable because tension and abrasion are two different mechanical
412 behaviors. In tension, ECC exhibits strain-hardening behavior through macroscopic
413 cracking, fiber bridging and pulling out from the matrix. On the other hand, abrasion
414 is a surface damage process with removal of materials in microscopic scale, while no
415 macroscopic cracking in tension occurred during this process (see Fig. 10). Therefore,
416 the energy absorbing capacity of ECC which is a tensile behavior has little effect on
417 its abrasion resistance. In Fig. 12, it shows that the index of the abrasion resistance is
418 a function of the fiber volume ratio of ECC specimens. As discussed above, the
419 abrasion resistance of ECC is dependent on the compressive and tensile strengths.
420 While as shown in Figs.7 and 8 (b), the compressive and tensile strengths of ECC are
421 associated with the fiber volume ratio. In other words, the fiber content of ECC has
422 obvious effect on its abrasion resistance. A fitting function based on the Gaussian
423 model of "f(x) = a1*exp(-((x-b1)/c1)^2) + a2*exp(-((x-b2)/c2)^2)" by MATLAB is
424 proposed to quantify the relationship between the index of abrasion resistance (I_a) of
425 ECC (in $(kr)^{1/2}$/mm) and its fiber volume ratio (x, in %):

$$I_a = 0.3\exp\left(-\left(\frac{x-2.6}{1.3}\right)^2\right) + 1.3\exp(-(\frac{x-49}{69})^2) \quad (4)$$

This function was developed by fitting the experimental data in Fig. 12. The predictions using this function agreed well with experimental results with a standard deviation of 0.01 and a COV of 0.01. This function can be used to predict the index of the abrasion resistance of ECC with a fiber volume ratio lower than 5%.

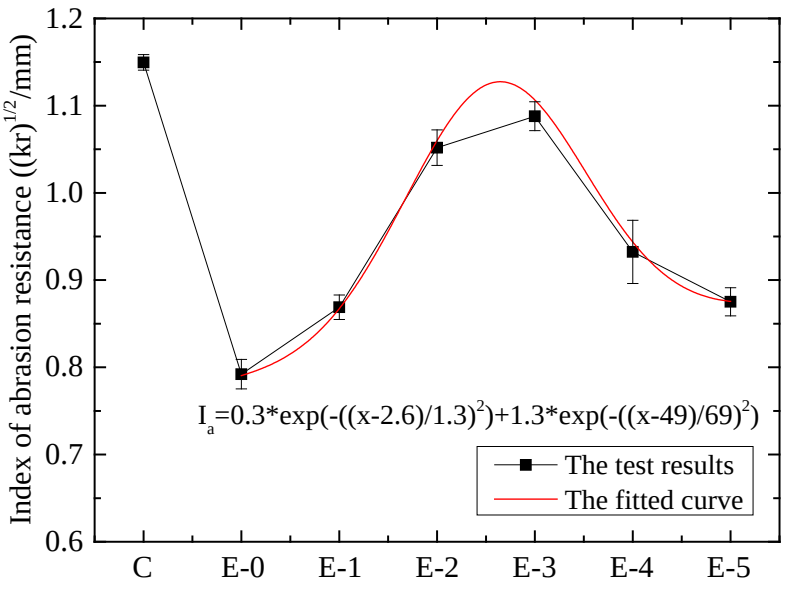

Fig. 12. The index of the abrasion resistance of the ECC and concrete specimens

3.3 The Acoustic Wave Attenuation of the ECC and Concrete Specimens

The acoustic wave attenuation of the ECC and concrete specimens were determined using Eq. 3 and plotted against the acoustic frequencies in Fig. 13. It can be seen that, for any acoustic frequency, the acoustic wave attenuation of the ECC and concrete specimens follow the same sequence of C≈E-0<E-1<E-2<E-3<E-4<E-5. It is interesting to notice that the acoustic wave attenuation of the ECC and concrete

specimens seem independent on the acoustic frequency. This observation can be explained using the wave length of the acoustic wave which is related to the wave speed and frequency [64]:

$$L = \mathrm{V}_{\text{acoustic wave}}/\mathrm{F} \quad (5)$$

where, L is the acoustic wavelength (m), $V_{acoustic\ wave}$ is the speed of the acoustic wave (346 m/s, 25℃), F is the acoustic frequency in Hz.

According to the Eq. 6, the acoustic wavelength ranges from 0.17 m to 1.73 m for the frequency from 200 Hz to 2000 Hz. The distance between the two receivers A and B was 35 mm (see Fig. 4) which was much shorter than the wavelengths of all the acoustic frequencies. Within such a short distance, the reflection and diffraction of the acoustic wave could hardly happen with a large proportion of the acoustic wave bypassed the specimen directly. Therefore, given the distance between the two receivers A and B was constant, the absorption of the acoustic waves with a frequency from 200 Hz to 2000 Hz would experience little change [43, 64].

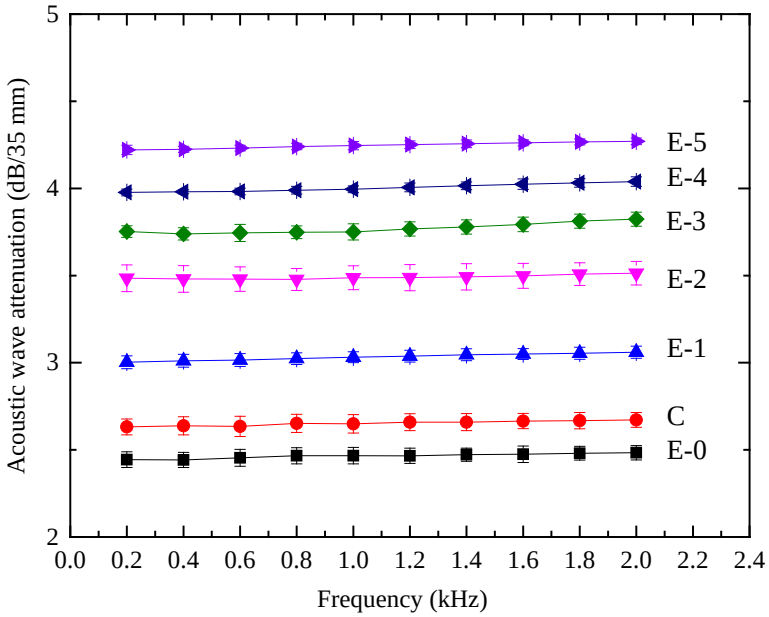

Fig. 13. The acoustic wave attenuation of the ECC and concrete specimens under various acoustic frequencies

The acoustic wave attenuation corresponding to the frequencies from 200 Hz to 2000 Hz for each specimen in Fig. 13 were averaged and plotted against the fiber content in Fig. 14. It is obvious that the acoustic wave attenuation is positively related to the fiber content of the ECC specimens. It was reported that the acoustic wave attenuation of a material is closely related to its void ratio [15]. Therefore, the void ratio measured in Section 3.1 was also plotted in Fig. 14. It is clear that the acoustic wave attenuation and the void ratio have the same trend as the function of the fiber content of the ECC specimens. It is easy to understand because higher void ratio means better acoustic insulation properties for a material. Similar to the index of the abrasion resistance, the acoustic wave attenuation (Δ, in dB/35 mm) of ECC can also be modeled based on "f(x) = ax+b" as a fitting function of the fiber volume fraction (*x*,

in %):

$$\Delta = 0.3x + 2.8 \quad (6)$$

The regressed line is plotted in Fig. 14 and compared with the experimental results. The predicted results by the regressed line agree well with the experimental data with a standard deviation of 0.14 and a COV of 0.04.

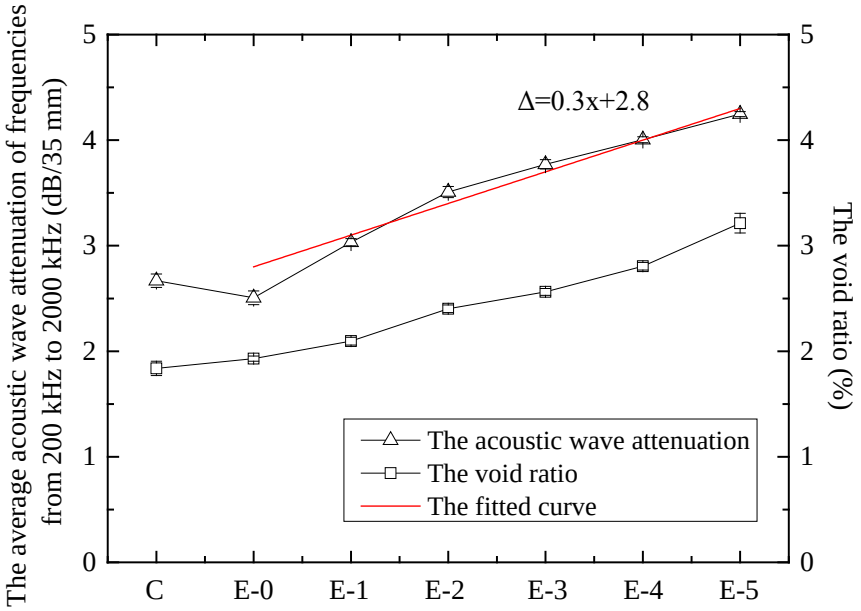

Fig. 14. The averaged acoustic wave attenuation of the ECC and concrete specimens and the fitted curve

This method could also be used to test the acoustic wave attenuation for noise pollution prevention at the actual airport pavement. The measuring instruments could be moved and operated conveniently. It should be noted that the surface of the test pavement need to be plain, so the acoustic sensors could generate and receive the acoustic wave well.

4. CONCLUSIONS

This paper investigated the abrasion resistance and the acoustic wave attenuation of the ECC with different fiber volume ratios. Ordinary concrete specimens were also tested for comparison purpose. The physical and mechanical properties of ECC and concrete specimens including compression strength, tensile stress-strain behaviors and the total void ratios were firstly tested. Abrasion tests were conducted and the index of abrasion resistance of ECC and concrete were measured. The acoustic wave attenuation of ECC and concrete with the acoustic frequency ranging from 200 Hz to 2200 Hz were characterized. Simple empirical equations were proposed for the prediction of the abrasion resistance and the acoustic wave attenuation of ECC as a function of the fiber volume ratio. Based on the research of this study, the following conclusions could be drawn:

(1) The compressive and tensile strengths of ECC can be affected by the fiber volume ratio. There exists an optimum fiber volume ratio for ECC to achieve the highest compressive and tensile strength, which is 3% in this paper. However, the strain-hardening behavior of ECC is independent of the fiber volume ratio and can only be achieved by careful calibration of the micro fracture mechanics. In this paper, only E-2 with 2% PVA fibers in volume ratio exhibited strain-hardening behavior.

(2) The void ratio of ECC is almost a linear function of the fiber volume ratio. This is because more voids can be generated when the interfaces between PVA fibers and surrounding matrix increase.

515 (3) The abrasion resistance of ECC is mainly dependent on the compressive and
516 tensile strengths, while the tensile strain-hardening behavior or the energy absorbing
517 capacity of ECC has little effect. It was found that ECC achieved the best abrasion
518 resistance with an index of 1.09 with a fiber volume ratio of 3%, which was very
519 close to that of concrete.
520 (4) The acoustic wave attenuation of ECC is independent of the acoustic wave
521 frequency, and linearly related to its void ratio. This indicates that ECC with more
522 PVA fibers has better noise absorption capacity when used as pavement material. It
523 should be noted that, the acoustic testing method in this paper is for the first time used
524 for the assessment of the noise prevention behavior of a material. Though
525 theoretically it is applicable, its reliability for such assessment should be validated by
526 ISO standards in [36-39].
527 (5) The abrasion resistance and the acoustic wave attenuation of ECC are all
528 functions of the fiber volume ratio. Empirical equations are proposed which agree
529 well with the experimental results. These two equations can be used to predict the
530 abrasion resistance and acoustic wave attenuation of ECC with a fiber volume ratio
531 lower than 5%, using the materials mentioned in this paper.
532 For the strain hardening ECC with a fiber volume ratio of 2% (E-2), it has
533 comparable compressive and tensile strengths to the ordinary concrete. The index of
534 the abrasion resistance of E-2 is 1.05, which is also close to the ordinary concrete.
535 More importantly, there is no stone debris generated during the abrasion process of
536 ECC which reduces the hazard to the road users. In addition, the acoustic wave

attenuation of the strain hardening ECC (2%) is 3.5 dB/35mm which suggests much better noise absorbing capacity than that of the ordinary concrete. Therefore, the experimental results in this paper prove that ECC is a desirable pavement material comparing to the ordinary concrete in terms of abrasion resistance and acoustic wave attenuation behaviors.

ACKNOWLEDGEMENT

The authors gratefully acknowledge the financial support provided by the National Science Foundation of China (51608020). This work was also funded by the Thousand Talents Plan (Young Professionals) in China. The authors would like to thank Associate Professor Juan Guan for providing the microscope facilities at the School of Materials Science and Engineering at Beihang University.

REFERENCES

[1] Ahmed I, Rahman MH, Seraj SM, Hoque AM. Performance of plain concrete runway pavement. Journal of Performance of Constructed Facilities, 1998; 12(3): 145-152.

[2] Smith KD, Roesler JR. Review of fatigue models for concrete airfield pavement design. Airfield Pavements: Challenges and New Technologies, 2004; 231-258.

[3] Giussani F, Mola F. Durable concrete pavements: The reconstruction of runway head 36R of Milano Linate International Airport. Construction and Building Materials, 2012; 34: 352-361.

[4] Ziari H, Hayati P, Sobhani J. Air-entrained air field self-consolidating concrete pavements: strength and durability. International Journal of Civil Engineering, 2017; 15(1): 21-33.

[5] Morgan D R. Compatibility of concrete repair materials and systems. Construction and building materials, 1996; 10(1): 57-67.

[6] Qian SZ, Li VC. Durable pavement with ECC. Proceedings of 1st International Conference on Microstructure Related Durability of Cementitious Composites, 2008; 535-543.

[7] Lepech MD, Li VC. Sustainable pavement overlays using engineered cementitious

568 composites. International Journal of Pavement Research and Technology, 2010; 3(5):
569 241-250.
570 [8] Qian SZ, Li VC, Zhang H, Keoleian GA. Life cycle analysis of pavement overlays
571 made with Engineered Cementitious Composites. Cement and Concrete Composites,
572 2013; 35(1): 78-88.
573 [9] Yucel HE, Guler M, Jashami H, Yaman IO, Sahmaran M. Thin ECC overlay
574 systems for rehabilitation of rigid concrete pavements. Magazine of Concrete
575 Research, 2013; 65(2): 108-120.
576 [10] Li VC. Tailoring ECC for special attributes: A review. International Journal of
577 Concrete Structures and Materials, 2012; 6(3): 135-144.
578 [11] Sahmaran M, Li VC. Durability of mechanically loaded engineered cementitious
579 composites under highly alkaline environments. Cement and Concrete Composites,
580 2008; 30(2): 72-81.
581 [12] Lepech MD, Li VC. Application of ECC for bridge deck link slabs. Materials and
582 Structures, 2009; 42(9): 1185-1195.
583 [13] Li B, Ke G, Zhou M. Influence of manufactured sand characteristics on strength and
584 abrasion resistance of pavement cement concrete. Construction and Building
585 Materials, 2011, 25(10): 3849-3853.
586 [14] Siddique R. Compressive strength, water absorption, sorptivity, abrasion resistance
587 and permeability of self-compacting concrete containing coal bottom ash.
588 Construction and Building Materials, 2013; 47: 1444-1450.
589 [15] Sandberg U. Low noise road surfaces. A state of the art review. Journal of the
590 Acoustical Society of Japan, 1999; 20(1): 1-17.
591 [16] Li M, Keulen WV, Ven MVD, Molenaar A, Tang G. Investigation on material
592 properties and surface characteristics related to tyre–road noise for thin layer
593 surfacings. Construction and Building Materials, 2014; 59: 62-71.
594 [17] Li VC. Bendable concrete. Innovation in Construction, 2016; 11-15.
595 [18] Qian SZ, Li VC, Zhang H, Keoleian GA. Life cycle analysis of pavement overlays
596 made with Engineered Cementitious Composites. Cement and Concrete Composites,
597 2013; 35(1): 78-88.
598 [19] Siddique R, Khatib JM. Abrasion resistance and mechanical properties of
599 high-volume fly ash concrete. Materials and Structures, 2010; 43(5): 709-718.
600 [20] Singh G, Siddique R. Abrasion resistance and strength properties of concrete
601 containing waste foundry sand (WFS). Construction and Building Materials, 2012;
602 28(1): 421-426.
603 [21] Laplante P, Aitcin PC, Vezina D. Abrasion resistance of concrete. Journal of
604 Materials in Civil Engineering, 1991; 3(1): 19-28.
605 [22] Rashad AM. A preliminary study on the effect of fine aggregate replacement with
606 metakaolin on strength and abrasion resistance of concrete. Construction and
607 Building Materials, 2013; 44: 487-495.
608 [23] Li B, Ke G, Zhou M. Influence of manufactured sand characteristics on strength and
609 abrasion resistance of pavement cement concrete. Construction and Building
610 Materials, 2011; 25(10): 3849-3853.
611 [24] Yen T, Hsu TH, Liu YW, Chen SH. Influence of class F fly ash on the

612 abrasion–erosion resistance of high-strength concrete. Construction and Building
613 Materials, 2007; 21(2): 458-463.
614 [25] Naik TR, Singh SS, Hossain MM. Abrasion resistance of concrete as influenced by
615 inclusion of fly ash. Cement and Concrete Research; 1994, 24(2): 303-312.
616 [26] Siddique R. Compressive strength, water absorption, sorptivity, abrasion resistance
617 and permeability of self-compacting concrete containing coal bottom ash.
618 Construction and Building Materials, 2013; 47: 1444-1450.
619 [27] Atic CD. High volume fly ash abrasion resistant concrete. Journal of Materials in
620 Civil Engineering, 2002; 14(3): 274-277.
621 [28] Siddique R, Kapoor K, Kadri EH, Bennacer R. Effect of polyester fibres on the
622 compressive strength and abrasion resistance of HVFA concrete. Construction and
623 Building Materials, 2012; 29: 270-278.
624 [29] Grdic ZJ, Curcic GAT, Ristic NS, Despotovic IM. Abrasion resistance of concrete
625 micro-reinforced with polypropylene fibers. Construction and Building Materials,
626 2012; 27(1): 305-312.
627 [30] Atis CD, Karahan O, Ari K, Sola ÖC, Bilim C. Relation between strength properties
628 (flexural and compressive) and abrasion resistance of fiber (steel and
629 polypropylene)-reinforced fly ash concrete. Journal of Materials in Civil
630 Engineering, 2009; 21(8): 402-408.
631 [31] Li VC. Progress and application of engineered cementitious composites. Journal of
632 the Chinese Ceramic Society, 2007; 35(4): 1-6.
633 [32] Lepech MD, Li VC. Sustainable pavement overlays using engineered cementitious
634 composites. International Journal of Pavement Research and Technology, 2010, 3(5):
635 241-250.
636 [33] Wu C, Li VC. CFRP-ECC hybrid for strengthening of the concrete structures.
637 Composite Structures, 2017, 187: 372-382.
638 [34] Wu C, Li VC. Thermal-mechanical behaviors of CFRP-ECC hybrid under elevated
639 temperatures. Composites Part B Engineering, 2017, 110: 255-266.
640 [35] Kamile TF, Burak F, Ravi R, Lee BY, Li VC. The role of flaw size and fiber
641 distribution on tensile ductility of PVA-ECC. Composites Part B Engineering, 2014,
642 56: 536-545.
643 [36] ISO 11819-1:1997. Acoustics - Measurement of the influence of road surfaces on
644 traffic noise - Part 1: Statistical Pass-By method. Switzerland: International
645 Organization for Standardization; 1997.
646 [37] ISO 11819-2:2017. Acoustics - Measurement of the influence of road surfaces on
647 traffic noise - Part 2: The close-proximity method. Switzerland: International
648 Organization for Standardization; 2017.
649 [38] ISO/TS 11819-3:2017. Acoustics - Measurement of the influence of road surfaces
650 on traffic noise - Part 3: Reference tyres. Switzerland: International Organization for
651 Standardization; 2017.
652 [39] ISO/PAS 11819-4:2013. Acoustics - Method for measuring the influence of road
653 surfaces on traffic noise - Part 4: SPB method using backing board. Switzerland:
654 International Organization for Standardization; 2013.
655 [40] Lin S, Hung W, Leng Z. Air pollutant emissions and acoustic performance of hot

mix asphalts. Construction and Building Materials, 2016; 129: 1-10.
[41] Chen J, Ren J, YIN TY. Nondestructive evaluation of notched cracks in mortars by nonlinear ultrasonic technique. Nondestructive Testing and Evaluation, 2016; 31(2): 109-121.
[42] Chen J, Wang H, Yao YP. Experimental study of nonlinear ultrasonic behavior of soil materials during the compaction. Ultrasonics, 2016; 69: 19-24.
[43] In CW, Kim JY, Kurtis KE, Jacobs LJ. Characterization of ultrasonic Rayleigh surface waves in asphaltic concrete. NDT&E International, 2009; 42(7): 610-617.
[44] Li VC. On engineered cementitious composites (ECC)-a review of the material and its applications. Journal of Advanced Concrete Technology, 2003; 1(3): 215-230.
[45] Wang S. Micromechanics based matrix design for engineered cementitious composites. University of Michigan, Ann Arbor, USA, 2005.
[46] Wu C. Micromechanical tailoring of PVA-ECC for structural applications. University of Michigan, Ann Arbor, USA, 2001.
[47] JGJ 55-2011. Specification for mix proportion design of ordinary concrete. Beijing: Ministry of housing and Urban-Rural development of the People's Republic of China; 2011.
[48] GB/T 50081-2002. Standard for test method of mechanical properties on ordinary concrete. Beijing: Ministry of housing and Urban-Rural development of the People's Republic of China; 2002.
[49] JSCE Concrete Committee. Recommendations for design and construction of high performance fiber reinforced cement composites with multiple fine cracks. Japan Society of Civil Engineers, Tokyo, 2008.
[50] GB/T 16925-1997. Test method for abrasion resistance of concrete and its products. Beijing: Ministry of housing and Urban-Rural development of the People's Republic of China; 1997.
[51] Yin TY Meng WL, Talebzadeh N, Chen J. Experimental characterization of sulfate damage of concrete based on the harmonic wave modulation technique. AIP Conference Proceedings, 2017; 1806(1): 080008.
[52] Rokugo K, Kanda T, Yokota H, Sakata N. Applications and recommendations of high performance fiber reinforced cement composites with multiple fine cracking (HPFRCC) in Japan. Materials and structures, 2009; 42(9): 1197-1208.
[53] Bhutta MAR, Tsuruta K. Evaluation of properties of workable porous concrete. Proceedings of the 35th Conference on Our World in Concrete & Structures, 2010: 2-11.
[54] Zheng H, Lin SQ. Ultrasonic testing. Beijing: China Labor Social Security Press, 2015.
[55] Naik TR. Concrete durability as influenced by density and/or porosity. Proceedings of the Cement and Concrete Institute of Mexico Symposium, Mexico, 1997: 4-7.
[56] Taylor HFW. Cement chemistry. London: Telford Publishing, 1997.
[57] Provis JL. Alkali activated materials: state-of-the-art report. Berlin: Springer Verlag, 2014.
[58] Akkaya Y, Peled A, Shah SP. Parameters related to fiber length and processing in cementitious composites. Materials and Structures, 2000; 33(8): 515-524.

[59] Sakulich AR, Li VC. Nanoscale characterization of engineered cementitious composites (ECC). Cement and Concrete Research, 2011; 41(2): 169-175.
[60] Ezeldin AS, Balaguru PN. Normal and high strength fiber reinforced concrete under compression. Journal of materials in civil engineering, 1992; 4(4): 415-429.
[61] Perez-Pena M, Mobasher B. Mechanical properties of fiber reinforced lightweight concrete composites. Cement and Concrete Research, 1994; 24(6): 1121-1132.
[62] Pacheco-Torgal F, Castro-Gomes J, Jalali S. Alkali-activated binders: A review: Part 1. Historical background, terminology, reaction mechanisms and hydration products. Construction and Building Materials, 2008; 22(7): 1305-1314.
[63] Hewlett P. Lea's chemistry of cement and concrete. Berlin: Springer Verlag, 2003.
[64] Du GH, Zhu ZM, Gong XF. Basic acoustics. Nanjing: Nanjing University Press, 2012.